World Journal of Advanced Engineering Technology and Sciences
eISSN: 2582-8266
Cross Ref DOI: 10.30574/wjaets
Journal homepage: https://wjaets.com/

(REVIEW ARTICLE)

Check for updates

Laboratory preparation of LSM and LSF sputtering targets using PTFE rings for deposition of SOFC thin film electrodes

Ramin Babazadeh Dizaj [1,*] and Nastaran Sabahi [2]

[1] *Center for Energy Storage Materials and Devices, Department of Metallurgical and Materials Engineering, Middle East Technical University, Ankara, Turkey.*
[2] *Department of Civil Engineering, Middle East Technical University, Ankara, Turkey.*

World Journal of Advanced Engineering Technology and Sciences, 2023, 10(02), 203–212

Publication history: Received on 12 November 2023; revised on 18 December 2023; accepted on 21 December 2023

Article DOI: https://doi.org/10.30574/wjaets.2023.10.2.0310

Abstract

The manufacturing of sputtering targets diverges from the conventional methods in ceramic processing, primarily because the quantities produced are frequently limited. The application of hot-press in this scenario significantly simplifies the sputter target fabrication process, allowing precise control over both target density and dimensions during pressing. However, without a hot press, the fabrication necessitates substantial preliminary efforts, which may be challenging to justify due to the restricted production volume. This study utilizes polytetrafluoroethylene (PTFE) rings as compaction dies filled with powders. Subsequently, the die is deformed between parallel platens, effectively compacting the powders. The method relies on the characteristic that the pressing results in minimal change in the internal diameter of the ring. This approach was exemplified through the creation of 2-inch ($La_{0.5}Sr_{0.5}$) $MnO_{3-\delta}$ (LSM) and ($La_{0.8}Sr_{0.2}$) $FeO_{3-\delta}$ (LSF) targets, where the deformable die was sized based on preliminary experiments involving smaller-diameter PTFE rings. The outcome of this fabrication process successfully produced sputter targets with high density, well within the tolerances of the sputter gun. Further tests involved using the prepared targets for the successful deposition of thin film LSM-LSF composite cathodes for SOFC applications.

Keywords: Sputter Targets; LSM; LSF; Deformable PTFE dies; Thin Film Cathodes; SOFC

1. Introduction

It is a commonly recognized truth that the sustainability of an ecosystem hinges on the incorporation of clean energy [1-7]. An influential strategy in the realm of clean energy involves the application of electrochemical conversion devices [8-10]. Among these devices, solid oxide fuel cells (SOFCs) emerge as standout performers [11, 12]. SOFCs excel in transforming the stored chemical energy in fuels like hydrogen and methane into electricity through electrochemical reactions on oxide materials [13-17]. Despite their operational resemblance to batteries, these conversion devices have the capability to continuously generate the required energy as long as a steady supply of fuel is provided [18-20].

Thin film oxides have been extensively investigated as electrode materials in devices for energy conversion and storage [21-24]. Among the various methods used to produce thin films, sputtering, a form of physical vapor deposition, has gained considerable attention in recent years [25, 26]. This technique involves ejecting atoms or molecules from a source material (the target) and depositing them onto a substrate to form a thin film [27-31]. Sputter targets, particularly those intended for research purposes, must meet specific criteria despite their relatively small size [29, 32-34]. Firstly, they must possess high relative densities, preferably exceeding 0.90, to prevent compositional discrepancies between the sputtered film and the target [35-38]. Additionally, they are expected to exhibit a uniform distribution of grain size to mitigate nodule formation issues that could arise during the deposition of films [39, 40].

* Corresponding author: Ramin Babazadeh Dizaj

It is standard practice to conduct thorough preliminary research to determine the fabrication parameters [41-44]. Once these parameters are identified, a die of appropriate dimensions is prepared, and the powders are compressed and sintered under carefully controlled conditions [45, 46]. In the case of sputter targets, the use of hot press significantly simplifies this process, ensuring controlled densification with proper dimensional precision [8, 47, 48]. In situations where the hot press is not available, one must resort to the conventional method of compression and sintering, which, as mentioned earlier, requires extensive preliminary work [49, 50]. This can be particularly demanding, especially in scenarios involving low-volume production [36, 51-54].

The present study is a component of a larger initiative aimed at creating a highly effective cathode material for Solid Oxide Fuel Cells (SOFCs) through the process of sputtering deposition. The objective is to generate sputter targets characterized by high density and a consistent grain size, suitable for depositing thin films intended for use in SOFC components such as $(La_{0.5}Sr_{0.5})MnO_{3-\delta}$ (LSM) and $(La_{0.8}Sr_{0.2})FeO_{3-\delta}$ (LSF). To achieve this goal, we employ a technique that involves the use of a deformable PTFE die for the compaction process.

2. Materials and Methods

$(La_{0.5}Sr_{0.5})MnO_{3-\delta}$ (LSM) and $(La_{0.8}Sr_{0.2})FeO_{3-\delta}$ (LSF) powders were synthesized using the Pechini method developed by M.P. Pechini in 1967. The precursors employed in this method were nitrates, $La(NO_3)_3.6H_2O$ (Alfa Aesar, 99.99%), $Sr(NO_3)_2$ (Alfa Aesar, 99%), $Mn(NO_3)_2.H_2O$ (Alfa Aesar, 98%), and $Fe(NO_3)_3.9H_2O$ (Alfa Aesar, 99.99%), used for the sol-gel preparation of LSM and LSF powders. In this process, the solution of the respective nitrates is mixed with ethylene glycol and citric acid by stirring at 100 °C for 20 minutes. After drying at 150 °C, calcination was carried out at 850 °C for 5 hours. Subsequently, the resulting powders underwent grinding in a mortar.

Compaction was performed at pressures ranging from 64 MPa to 121 MPa, using dies with a 56 mm inner diameter, a 5 mm wall thickness, and a 5 mm height, as shown in Figure 1 (a). The compacts were then sintered at selected temperatures between 1300 and 1500 °C. This process resulted in sputter target discs slightly larger than 2 inches in diameter, which were subsequently ground down to a 2-inch diameter.

Regular utilization of conventional sputter targets can result in the formation of cracks caused by repeated exposure to electrical power and environmental influences. This cycle persists until the target ultimately fractures and turns into a powder. To address this problem and ensure optimal contact between the target material and the gun, we have introduced a copper holder (as illustrated in Figure 1 (b)), where the finished target is positioned to prevent cracking and preserve its integrity.

Figure 1 (a) PTFE deformable die rings, used for the pressing of the targets. On the left-hand side, the ring before pressing, and the right-hand side corresponds to the ring after pressing the powder. (b) Copper holder used as a protective and provider of enhanced contact between target and sputtering gun

Sputter deposition was conducted in a specialized system tailored for combinatorial thin film research, incorporating radio frequency (R.F.) sputter guns. The target holders, measuring 2 inches in diameter with a copper base, allowed for the attachment of targets using a 49 mm inner diameter ring that could be securely fastened onto the base. This configuration facilitated the use of targets with a diameter of 50 mm, within tolerances of ± 0.7 mm.

Structural characterization was performed through X-ray diffraction using the D/MAX-2200 Rigaku X-Ray diffractometer. The scanning rate was set at 2 °/min, utilizing Cu-Kα radiation. When necessary, refinement of X-ray data was carried out using MAUD software (Lutterotti et al. 2000). Microstructural observations were conducted with the FEI Nova Nano-SEM 430, and chemical analyses, as needed, were determined using the EDS detector.

3. Results and Discussion

Compaction dies are usually created by machining tool steels with close tolerances, and then undergoing quenching and tempering. This manufacturing process is quite complex, and a more straightforward option would be highly advantageous. As an alternative, we propose utilizing a deformable die.

Deformable dies employed in the production of LSF and LSM targets have a ring-shaped configuration with a low aspect ratio, meaning the height is significantly smaller than the diameter, as depicted in Figure 1 (a). To conserve powder during preliminary experiments, small diameter dies were utilized, involving the machining of numerous PTFE rings with a 20 mm inner diameter from suitable PTFE rod diameters.

The procedures outlined for the conventional die in target fabrication were replicated using a 20 mm PTFE die, where compaction pressure ranged from 50 to 135 MPa. It's important to note that the compaction geometry differs from conventional practices in this context. The PTFE ring is compressed between two parallel platens, causing deformation of the ring and compaction of the powder. Consequently, the ring is employed once and then discarded. This stands in contrast to conventional compaction, where powders are compacted within a die–punch system, a process that can be iterated multiple times with the same toolset, as illustrated in Figure 2.

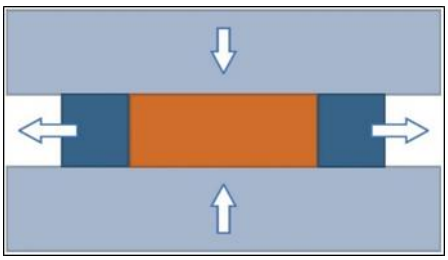

Figure 2 Schematic representation of the powder pressing method using PTFE rings. By applying pressure over powder and ring, the powder is pressed, and the die is deformed

In the trials, PTFE rings were filled with powder and subjected to tapping to achieve consistent density. Subsequently, they were uniaxially pressed to the predetermined compaction pressure. Throughout the pressing process, the PTFE rings experienced a reduction in height, accompanied by radial flow. Notably, there was minimal alteration in the inner diameter of the ring, and the diameters of the green pellets measured across five experiments remained within 20.2 mm.

Considering this observation, PTFE rings of appropriate sizes were prepared. The die was filled with powder and compacted, resulting in a sintered compact under the same conditions. The resulting sputter target exhibited a high level of density, with the diameter of the sintered oxide measuring 50.5 mm ± 0.3 mm, falling within the tolerances of the sputter gun holder.

The thin film cathode, measuring 2.7 mm in thickness and manufactured through this process, underwent testing for its deposition capabilities. The target was loaded onto the holder and exhibited sufficient flatness, eliminating the need for a backing layer. Sputtering was conducted over a 16-hour period with an argon flow maintained at a pressure of 5 mTorr. The substrate used was a Scandium-Stabilized Zirconia (ScSZ) disc, resulting in a satisfactory thin film cathode with a thickness of 460 nm. The film demonstrated uniformity and was free of voids, as depicted in Figure 8. Notably, films co-sputtered using two targets, LSM and LSF, both fabricated with deformable dies, were produced and electrochemically tested, yielding highly satisfactory results.

The method outlined in this study is practical and streamlines the production of sputter targets or similar products. It's noteworthy that the applicability of this approach stems from the minimal alteration in the inner diameter of the PTFE die during pressing. This phenomenon likely arises from the restriction of radial powder flow caused by friction between the powder and the platen. Consequently, this approach is well-suited for thin products, as an increase in height could lead to radial powder flow away from the platen. Estimating the limiting value of the diameter-to-height ratio proves challenging. It's essential to highlight that, particularly with particulate materials, friction in radial flow is higher away from the platens. These observations suggest that, for the given geometry and particulate materials, compaction predominantly occurs in the axial direction rather than the radial direction.

LSM Target: LSM powder was synthesized by utilizing precursors with specified amounts, as outlined in Table 1. Figure 3 displays the X-ray diffraction (XRD) pattern, while Figure 4 presents the refinement of the obtained powder. The peak positions align with JCPDC card No. 01-077-4313, and Rietveld refinement was performed using a CIF file (Kubota et al., 2000) to achieve a complete fit with LSM.

Following the calcination process at 800 °C for 5 hours, the resulting LSM powder underwent a comprehensive elemental distribution analysis through Energy Dispersive X-ray Spectroscopy (EDS). Table 2 provides the EDS analysis results for LSM calcined at 800 °C for 5 hours, averaged across five different locations. The lattice constants for the resultant LSM powder provided in Table 5.

Table 1 Composition of the precursors used for (La0.5Sr0.5)MnO3-δ Synthesis

$(La_{0.5}Sr_{0.5})MnO_{3-\delta}$ (M=216.2 gr/m)	**Molar Mass (M)**	**Amount (gr)**	**Mole**
$La(NO_3)_3.6H_2O$	433.10	3.77	0.0087
$Sr(NO_3)_2$	211.63	1.84	0.0087
$Mn(NO_3)_2.6H_2O$	286.95	5.00	0.0174
Citric Acid	192.12	20.08	0.1045
Ethylene glycol	62.07	25.95	0.4181

Table 2 Average values of EDS Analysis for LSM powder calcined at 800 °C for 5 hours

LSM $(La_{0.5}Sr_{0.5})MnO_{3-\delta}$	**Measured at%**
La	26.5
Sr	26.5
Mn	47

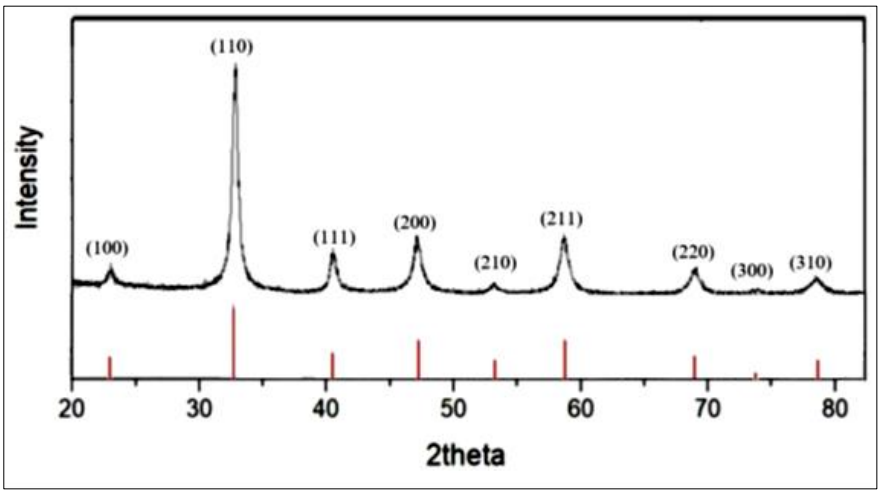

Figure 3 XRD pattern of LSM calcined at 800 °C for 5 hours

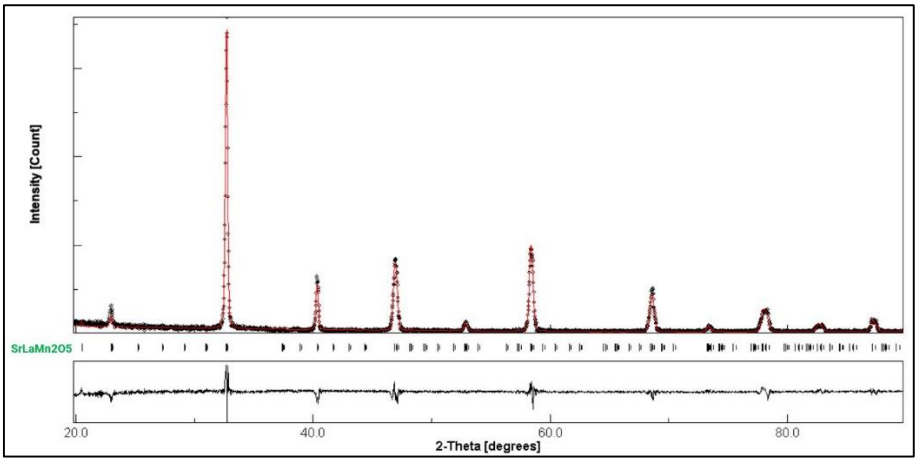

Figure 4 Rietveld refined XRD pattern of LSM calcined at 800 °C

As previously mentioned, powders were compressed utilizing a deformable Teflon die. Following initial trials, LSM powders were compressed at 140 MPa using a Teflon die with dimensions of 56 mm in diameter, 5 mm in height, and a wall thickness of 5 mm. Subsequently, the compact underwent sintering at 1500 °C for 3 hours, resulting in an approximate shrinkage of 10%, with the diameter reducing to about 52 mm. The resulting target was meticulously ground to achieve a diameter within the range of 50 to 51 mm. The sputter target produced is depicted in Figure 7 (a).

LSF Target: The X-ray diffraction (XRD) pattern obtained from the generated powder is depicted in both Figure 5 and Figure 6. The peak positions closely correspond to those of LSF (JCPDS Card No. 00-035-1480). Employing a CIF file (Jennings et al., 2003), the pattern underwent meticulous Rietveld refinement to ensure a thorough conformity with the standard LSF. The resulting lattice constants from this refinement are outlined in Table 5. Subsequent to the calcination process at 800 °C for 5 hours, an extensive Energy Dispersive X-ray Spectroscopy (EDS) analysis was conducted on the LSF powder. Table 4 presents the averaged EDS analysis outcomes for LSF calcined at 800 °C for 5 hours, derived from five distinct locations.

Table 3 Composition of the precursors used for (La0.8Sr0.2)FeO3-δ Synthesis

$(La_{0.8}Sr_{0.2})FeO_{3-\delta}$ (M=232.5 gr/m)	**Molar Mass (M)**	**Amount (gr)**	**Mole**
$La(NO_3)_3.6H_2O$	433.10	1.84	0.0042
$Sr(NO_3)_2$	211.63	0.22	0.00105
$Fe(NO_3)_3.9H_2O$	404.00	2.121	0.00525
Citric Acid	192.12	50.95	0.2424
Ethylene glycol	62.07	60.00	0.9699

Table 4 Average values of EDS Analysis for LSF powder calcined at 800 °C for 5 hours

$(La_{0.8}Sr_{0.2})FeO_{3-\delta}$	**Measured at%**
La	41.0
Sr	10.4
Mn	48.6

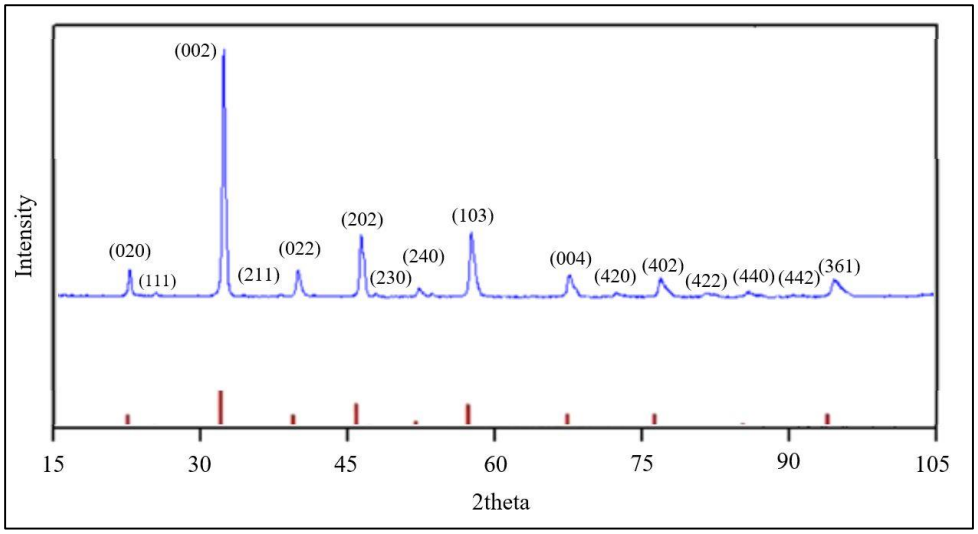

Figure 5 XRD pattern of LSF calcined at 800 °C for 5 hours

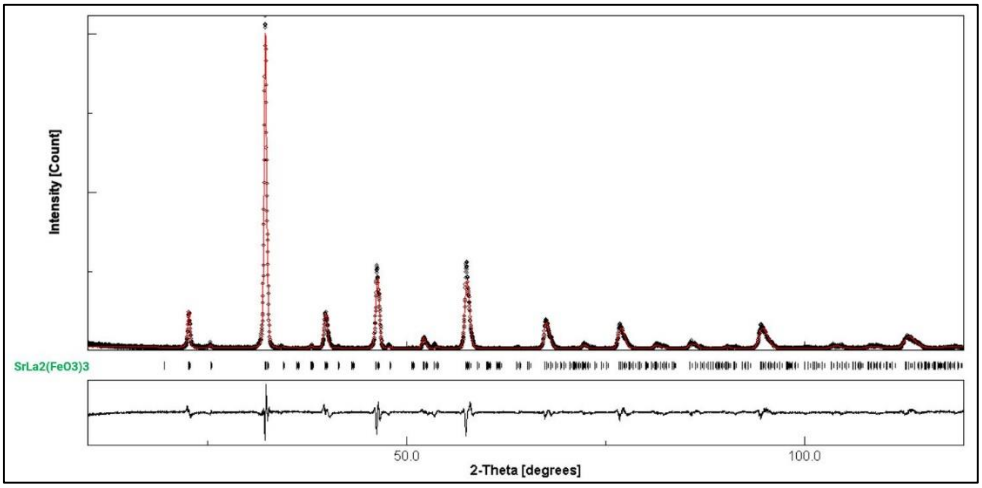

Figure 6 Rietveld refined XRD pattern of LSF calcined at 800 °C

Table 5 Lattice constants of LSF and LSM powders calcined at 800 °C for 5 hours

Material	a	b	c
LSM	5.445	5.445	7.759
LSF	5.536	7.836	5.550

Drawing from initial experiments, LSF powders underwent compression at a pressure of 140 MPa. The flexible die utilized had dimensions of 65 mm in diameter, 5 mm in height, and a wall thickness of 5 mm. Sintering was executed at 1500 °C for a duration of 5 hours, resulting in a radial shrinkage of the powders amounting to 27%. The ensuing disc was meticulously ground to achieve a diameter within the range of 50-51 mm, as depicted in Figure 7 (b).

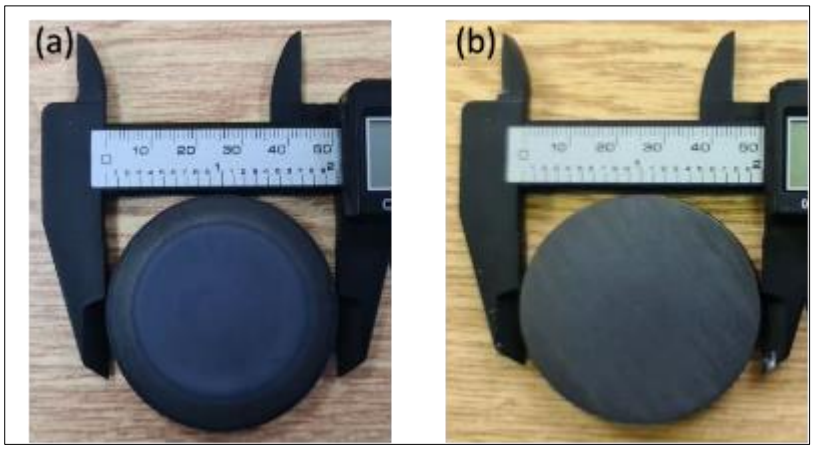

Figure 7 Prepared (a) LSM, (b) LSF sputtering targets after pressing and sintering

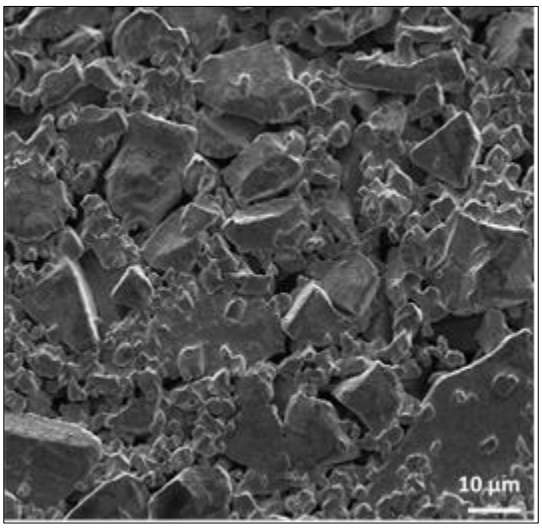

Figure 8 Top view scanning electron microscopy image of the LSM-LSF composite thin film deposited on ScSZ substrates using the prepared LSM and LSF sputtering targets

The aforementioned considerations might suggest that employing a PTFE die is not limited exclusively to products with a circular cross-section. If the previously discussed arguments regarding the constrained material flow in the radial direction hold true, then it's plausible to produce flat products of irregular shape, given a reasonable diameter-to-height ratio, using the same approach.

4. Conclusion

In this research, a straightforward technique has been proposed for producing flat ceramic items with a reduced aspect ratio. The method involves employing a deformable die, which can be fabricated from thermoplastic polymers or similar deformable materials. The die is filled with powders of uniform density achieved through tapping, and then compressed between parallel platens, compacting the powders while deforming the die. Prior to actual production, it proves beneficial to conduct tests using smaller diameter dies to collect data on sintered density and shrinkage in relation to the applied compaction pressure. The deformable die is then sized based on extrapolating the relevant data. This methodology was demonstrated through the fabrication of 2-inch $(La_{0.5}Sr_{0.5})MnO_{3-\delta}$ (LSM) and $(La_{0.8}Sr_{0.2})FeO_{3-\delta}$ (LSF) targets. The outcome of this fabrication process successfully produced sputter targets with high density, well within the tolerances of the sputter gun. Subsequent tests encompassed employing the fabricated targets to effectively deposit thin film LSM-LSF composite cathodes designed for applications in Solid Oxide Fuel Cells (SOFCs). The production of flat items with irregular shapes may also be achievable using the same method. Determining the maximum allowable height for the product is challenging, but it may not necessarily be minimal.

Compliance with ethical standards

Acknowledgments

The author would like to thank the Center for Energy Storage Materials and Devices at the Middle East Technical University. This study did not receive funding from any government or private agency.

Disclosure of conflict of interest

The author has no conflict of interest in this study.

References

[1] Alvandifar N, Saffar-Avval M, Amani E, Mehdizadeh A, Ebrahimipour M, Entezari S, et al. Experimental study of partially metal foam wrapped tube bundles. International Journal of Thermal Sciences. 2021, 162:106798.

[2] Bhuvela P, Taghavi H, Nasiri A, editors. Design Methodology for a Medium Voltage Single Stage LLC Resonant Solar PV Inverter. 2023 12th International Conference on Renewable Energy Research and Applications (ICRERA), 2023: IEEE.

[3] Kumar P, Jena P, Patro P, Lenka R, Sinha A, Singh P, et al. Influence of lanthanum doping on structural and electrical/electrochemical properties of double perovskite Sr2CoMoO6 as anode materials for intermediate-temperature solid oxide fuel cells. ACS applied materials & interfaces. 2019, 11(27):24659-67.

[4] Lee KT, Wachsman ED. Role of nanostructures on SOFC performance at reduced temperatures. Mrs Bulletin. 2014, 39(9):783-91.

[5] Nejatbakhsh S, Soodmand AM, Azimi B, Farshchi ME, Aghdasinia H, Kazemian H. Semi-pilot scale fluidized-bed reactor applied for the Azo dye removal from seawater by granular heterogeneous fenton catalysts. Chemical Engineering Research and Design. 2023, 195:1-13.

[6] Raghu S, Rajabi R, James R, Huang K, Khan JA, editors. Performance Comparison of Thermal Management Systems for Battery Packs Based on Numerical Simulation. Heat Transfer Summer Conference, 2023: American Society of Mechanical Engineers.

[7] Rostaghi Chalaki H, Babaei A, Ataie A, Seyed-Vakili SV. LaFe 0.6 Co 0.4 O 3 promoted LSCM/YSZ anode for direct utilization of methanol in solid oxide fuel cells. Ionics. 2020, 26:1011-8.

[8] Athari M-J, Tahmasebpoor M, Azimi B, Heidari M, Pevida C. Waste oleaster seed-derived activated carbon mixed with coarse particles of fluid catalytic cracking as a highly-efficient CO2 adsorbent at low temperatures. Process Safety and Environmental Protection. 2023, 178:580-94.

[9] Jiang S, Wang W, Zhen Y. Performance and electrode behaviour of nano-YSZ impregnated nickel anodes used in solid oxide fuel cells. Journal of power sources. 2005, 147(1-2):1-7.

[10] Lee JJ, Kim K, Kim KJ, Kim HJ, Lee YM, Shin TH, et al. In-situ exsolution of Ni nanoparticles to achieve an active and stable solid oxide fuel cell anode catalyst on A-site deficient La0. 4Sr0. 4Ti0. 94Ni0. 06O3-δ. Journal of Industrial and Engineering Chemistry. 2021, 103:264-74.

[11] Chalaki HR, Babaei A, Ataie A, Seyed-Vakili S-V, editors. The Effect of Impregnation of Ceramic Nano-particles on the Performance of LSCM/YSZ Anode Electrode of Solid Oxide Fuel Cell. 5th International Conference on Materials Engineering and Metallurgy, 2016.

[12] Jiang SP, Chen X, Chan S, Kwok J, Khor K. (La0. 75Sr0. 25)(Cr0. 5Mn0. 5) O3/YSZ composite anodes for methane oxidation reaction in solid oxide fuel cells. Solid State Ionics. 2006, 177(1-2):149-57.

[13] Aminnia N. CFD-XDEM coupling approach towards melt pool simulations of selective laser melting. 2023.

[14] Kaveh A, Almasi P, Khodagholi A. Optimum design of castellated beams using four recently developed meta-heuristic algorithms. Iranian Journal of Science and Technology, Transactions of Civil Engineering. 2023, 47(2):713-25.

[15] Mahato N, Banerjee A, Gupta A, Omar S, Balani K. Progress in material selection for solid oxide fuel cell technology: A review. Progress in Materials Science. 2015, 72:141-337.

[16] Mobli M, Farouk T, editors. High pressure micro glow discharge: Detailed approach to gas temperature modeling. APS Annual Gaseous Electronics Meeting Abstracts, 2014.

[17] Rajabi R, Dehwah AH, Krarti M. Impact of Dynamic Slab Insulation on Energy Performance of Residential Buildings. Journal of Engineering for Sustainable Buildings and Cities. 2022, 3(4):041001.

[18] Aminnia N, Adhav P, Darlik F, Mashhood M, Saraei SH, Besseron X, et al. Three-dimensional CFD-DEM simulation of raceway transport phenomena in a blast furnace. Fuel. 2023, 334:126574.

[19] Mahamud R, Mobli M, Farouk TI, editors. Modes of oscillation in a high pressure microplasma discharges. 2014 IEEE 41st International Conference on Plasma Sciences (ICOPS) held with 2014 IEEE International Conference on High-Power Particle Beams (BEAMS), 2014: IEEE.

[20] Rath MK, Lee K-T. Superior electrochemical performance of non-precious Co-Ni-Mo alloy catalyst-impregnated Sr2FeMoO6-δ as an electrode material for symmetric solid oxide fuel cells. Electrochimica Acta. 2016, 212:678-85.

[21] Aminnia N, Estupinan Donoso AA, Peters B. Developing a DEM-Coupled OpenFOAM solver for multiphysics simulation of additive manufacturing process. Scipedia com. 2022.

[22] Namazi H, Perera LP, editors. Trustworthiness Evaluation Framework for Digital Ship Navigators in Bridge Simulator Environments. International Conference on Offshore Mechanics and Arctic Engineering, 2023: American Society of Mechanical Engineers.

[23] Namazi H, Taghavipour A. Traffic flow and emissions improvement via vehicle-to-vehicle and vehicle-to-infrastructure communication for an intelligent intersection. Asian Journal of Control. 2021, 23(5):2328-42.

[24] Shirvani SMN, Gholami M, Afrasiab H, Talookolaei RAJ. Optimal design of a composite sandwich panel with a hexagonal honeycomb core for aerospace applications. Iranian Journal of Science and Technology, Transactions of Mechanical Engineering. 2023, 47(2):557-68.

[25] mahmoodreza Hashemi S, Aminnia N, Derakhshan S. Optimization Design of Pumps as Turbines (PATs) Arrays in a Water Distribution Network Aiming Energy Recovery.

[26] Marina OA, Canfield NL, Stevenson JW. Thermal, electrical, and electrocatalytical properties of lanthanum-doped strontium titanate. Solid State Ionics. 2002, 149(1-2):21-8.

[27] Mobli M. Thermal analysis of high pressure micro plasma discharge. 2014.

[28] Rajabi R, Raghu S, James R, Huang K, Khan JA, editors. PERFORMANCE COMPARISON OF BATTERY THERMAL MANAGEMENT SYSTEMS BASED ON NUMERICAL SIMULATION. ASTFE Digital Library, 2023: Begel House Inc.

[29] Rajabi R, Sun S, Billings A, Mattick VF, Khan J, Huang K. Insights into Chemical and Electrochemical Interactions between Zn Anode and Electrolytes in Aqueous Zn− ion Batteries. Journal of The Electrochemical Society. 2022, 169(11):110536.

[30] Seyed Mostafa Nasrollahpour Shirvani MG, Hamed Afrasiab, Ramazanali Jafari Talookolaei. Optimization of a Composite Sandwich Panel with Honeycomb Core Under Out-of-Plane Pressure with NMPSO Algorithm. The 28th Annual International Conference of Iranian Society of Mechanical Engineers (ISME)2020.

[31] Yang G, El Loubani M, Chalaki HR, Kim J, Keum JK, Rouleau CM, et al. Tuning Ionic Conductivity in Fluorite Gd-Doped CeO2-Bixbyite RE2O3 (RE= Y and Sm) Multilayer Thin Films by Controlling Interfacial Strain. ACS Applied Electronic Materials. 2023, 5(8):4556-63.

[32] Mobli M. Characterization Of Evaporation/Condensation During Pool Boiling And Flow Boiling: University of South Carolina, 2018.

[33] Rajabi R, Sun S, Huang K, editors. Performance Comparison of Three Polymer Electrolytes for Zinc Ion Batteries. 243rd ECS Meeting with the 18th International Symposium on Solid Oxide Fuel Cells (SOFC-XVIII), 2023: ECS.

[34] Salmasi F, Sabahi N, Abraham J. Discharge coefficients for rectangular broad-crested gabion weirs: experimental study. Journal of Irrigation and Drainage Engineering. 2021, 147(3):04021001.

[35] Aminnia N, Estupinan Donoso AA, Peters B. CFD-DEM simulation of melt pool formation and evolution in powder bed fusion process. 2022.

[36] Mobli M, Li C, editors. On the heat transfer characteristics of a single bubble growth and departure during pool boiling. International Conference on Nanochannels, Microchannels, and Minichannels, 2016: American Society of Mechanical Engineers.

[37] Shen J, Chen Y, Yang G, Zhou W, Tadé MO, Shao Z. Impregnated LaCo0. 3Fe0. 67Pd0. 03O3-δ as a promising electrocatalyst for "symmetrical" intermediate-temperature solid oxide fuel cells. Journal of Power Sources. 2016, 306:92-9.

[38] Shirvani SMN, Nakhi A, Karimi A, Mobli M. Optimizing methane direct utilization: The advanced Sr2CoMoO6-δ anode. 2023.

[39] Nakhi A, Mostafa S, Karimi A, Mobli M. Unveiling the Promoted LSTM/YSZ Composite Anode for Direct Utilization of Hydrocarbon Fuels. International Journal of Science and Engineering Applications. 2023, 12(12):18 - 24.

[40] Rajabi R, Thompson J, Krarti M. Benefit Cost Analysis of Electrification of Urban Districts: Case Study of Philadelphia, Pennsylvania. Journal of Engineering for Sustainable Buildings and Cities. 2020, 1(4):041004.

[41] Dizaj RB, Sabahi N. Optimizing LSM-LSF composite cathodes for enhanced solid oxide fuel cell performance: Material engineering and electrochemical insights. 2023.

[42] Mobli M, Mahamud R, Farouk T, editors. High pressure micro plasma discharge: Effect of conjugate heat transfer. 2013 19th IEEE Pulsed Power Conference (PPC), 2013: IEEE.

[43] Taghavi H. Liquid Cooling System for a High Power, Medium Frequency, and Medium Voltage Isolated Power Converter [M.S.]. United States -- South Carolina: University of South Carolina, 2023.

[44] Taghavi H, El Shafei A, Nasiri A, editors. Liquid Cooling System for a High Power, Medium Frequency, and Medium Voltage Isolated Power Converter. 2023 12th International Conference on Renewable Energy Research and Applications (ICRERA), 2023: IEEE.

[45] Aminnia N, Shateri M, Gheibi S, Torabi F. Modeling of Two-Phase flow in the Cathode Gas Diffusion Layer to Investigate Its Effects on a PEM Fuel Cell.

[46] Soodmand AM, Azimi B, Nejatbakhsh S, Pourpasha H, Farshchi ME, Aghdasinia H, et al. A comprehensive review of computational fluid dynamics simulation studies in phase change materials: applications, materials, and geometries. Journal of Thermal Analysis and Calorimetry. 2023, 148(20):10595-644.

[47] Babazadeh Dizaj R. DEVELOPMENT OF LSF-BASED DUAL-PHASE CATHODES FOR INTERMEDIATE TEMPERATURE SOLID OXIDE FUEL CELLS: Middle East Technical University, 2022.

[48] Su C, Wang W, Liu M, Tadé MO, Shao Z. Progress and prospects in symmetrical solid oxide fuel cells with two identical electrodes. Advanced Energy Materials. 2015, 5(14):1500188.

[49] Estupinan Donoso AA, Aminnia N, Peters B, Michels A. On the Reduction of Computational Costs for Tungsten Powder Bed Processes. 2022.

[50] Sun S, Wen Y, Billings A, Rajabi R, Wang B, Zhang K, et al. Protecting Zn Anode by Atomic Layer Deposition of ZrO2 to Extend the Lifetime of Aqueous Zn-ion Batteries. Energy Advances. 2023.

[51] Aminnia N, Peters B, ESTUPINAN AA. Multi-Scale Modeling of Melt Pool Formation and Solidification in Powder Bed Fusion: A Fully Coupled Computational Fluid Dynamics-Extended Discrete Element Method Approach. Available at SSRN 4502227.

[52] Taghavi M, Gharehghani A, Nejad FB, Mirsalim M. Developing a model to predict the start of combustion in HCCI engine using ANN-GA approach. Energy Conversion and Management. 2019, 195:57-69.

[53] Taghavi M, Perera LP, editors. Data Driven Digital Twin Applications Towards Green Ship Operations. International Conference on Offshore Mechanics and Arctic Engineering, 2022: American Society of Mechanical Engineers.

[54] Taghavi M, Perera LP, editors. Multiple Model Adaptive Estimation Coupled With Nonlinear Function Approximation and Gaussian Mixture Models for Predicting Fuel Consumption in Marine Engines. International Conference on Offshore Mechanics and Arctic Engineering, 2023: American Society of Mechanical Engineers.